Advanced Ceramics Progress: Vol. 8, No. 1, (Winter 2022) 27-35

Materials and Energy Research Center
MERC

Contents lists available at ACERP

Advanced Ceramics Progress

Journal Homepage: www.acerp.ir

Original Research Article

Characterization of Iranian Ancient Colored Glazed Ceramic Tiles of Safavid Era

Javad Fahim [a], Ebrahim Ghasemi [b,*], Maryam Hosseini Zori [c]

[a] *PhD, Department of Mechanical Engineering, Faculty of Mechatronics, Karaj Branch, Islamic Azad University, Karaj, Alborz, Iran*
[b] *Associate Professor, Department of Inorganic Pigments and Glazes, Faculty of Dyes and Pigments, Institute for Color Science and Technology (ICST), Tehran, Tehran, Iran*
[c] *Assistant professor, Department of Inorganic Pigments and Glazes, Faculty of Dyes and Pigments, Institute for Color Science and Technology (ICST), Tehran, Tehran, Iran*

* Corresponding Author Email: eghasemi@icrc.ac.ir (E. Ghasemi)

URL: https://www.acerp.ir/article_151935.html

ARTICLE INFO

Article History:

Received 1 May 2022
Received in revised form 17 June 2022
Accepted 19 June 2022

Keywords:

Egyptian Green
Safavid Era
Glazed Ceramics
Tiles
Copper

ABSTRACT

Investigation of the chemical compositions of pigments in glazed ancient ceramic tiles is of great importance from the monuments restoration point of view. In this regard, the current research aimed to investigate the chemical compositions and color charactristics of pigments in six glazed ancient ceramic tiles (Samples B1-B6) collected from Abdolazim Hasani Shrine (Safavid era), Ray, Iran. The results from X-ray Probe Micro Analyzer (XPMA), X-Ray Diffraction (XRD) patterns, and Energy Dispersive X-ray Spectroscopy (EDS) spectra revealed that the glazes were silica-based, containing 38.85 to 50.89 wt. % silicon in Samples B3 and B1, respectively, with lime, quarts, wollastonite, and cristobalite as the main phases. Raman spectroscopy also confirmed the presence of quartz, wollastonite, and tridymite along with chalk, gypsum, calcite, copper oxide, and green earth. The particle sizes of the pigments measured through Scanning Electron Microscopy (SEM) varied from 0.6 µm in Sample B1 to 5.5 µm in Sample B3. High intensity reflectance was also observed in the range of 490-560 nm, confirming the green color of the samples with different shades. In addition, CIE L*a*b* parameters clearly showed the correlation between the green color and concentration of Cu^{2+} ions within the silica-rich amorphous phase. Therefore, the presence of wollastonite, tridymite, and copper oxide in the samples under study was obviously indicative of presence of Egyptian green pigments in the glazes.

https://doi.org/10.30501/acp.2022.339876.1088

1. INTRODUCTION

Undoubtedly, Safavid era in Iran (1501-1732) is known as a period of shiny colored ceramic glazes in the world. However, the history of colored glazes dates back to ancient Egypt 4000 BC [1]. The variety of colors and geometries of the tiles flourished in the Safavid era. Unfortunately, there are very few limited papers of references investigating the compositions, colors, and glazes of ceramic tiles from the Safavid heritage. Most glazed ceramics inherited from the ruling period of Safavid dynesty are in blue or green-blue color.

Throughout the old kingdom (2600BC), Egyptian artisans fabricated a blue pigment, called the Egyptian blue, which is a mixture of calcium, silicon, and copper along with a soda flux. This pigment was used instead of

Please cite this article as: Fahim, J., Ghasemi, E., Hosseini Zori, M., "Characterization of Iranian Ancient Colored Glazed Ceramic Tiles of Safavid Era", ***Advanced Ceramics Progress***, Vol. 8, No. 1, (2022), 27-35. https://doi.org/10.30501/acp.2022.339876.1088

lapis-lazuli all around the Mediterranean region. However, the fabrication technology of the menyioned pigment was lost after the seventh century AD [2]. On the contrary, the synthetic pigment called the Egyptian green was produced from different proportions of the same components used for fabricating the Egyptian blue pigment [3–6]. As known, the diversity of production conditions (firing temperature, atmosphere, and cooling rate [6]) significantly affects the resulting properties of the pigment; however, a silicate enriched compound is expected as a final product. There are no ancient recipes available for the production of this green pigment [5]. Pagés-Camagna et al. [6] identified this type of pigment in a number of ceramic tiles from the Old Kingdom (3rd Millennium BCE) to the 21st Dynasty (10th Century BCE). Ullrich [7] discovered the Egyptian Green color on the bust of Nefertiti excavated at Tell el Amarna in the Tomb of Tutankhamen.

Bianchetti et al. [8] studied the fabrication of Egyptian blue and green frit using pure chemicals and natural raw Egyptian materials under different experimental conditions. They also pointed to the dependency of the recorded colors on the chemical composition and melting conditions.

A number of researchers produced a green pigment similar to para-wollastonite ($CaSiO_3$) together with a copper-bearing glass phase by altering the fabrication conditions to obtain Egyptian blue and subsequently Egyptian green [3-6]. Egyptian green (green frit) is a heterogeneous material characterized by the presence of para-wollastonite which is stable at 950-1150 °C [9]. It is a complex pigment which is usually obtained from Egyptian blue pigment $CaCuSi_4O_{10}$ (cuprorivaite) by heating CuO, $CaCO_3$, SiO_2, and Na_2CO_3 at the tempratures above 1000 ºC [10].

Pagés-Camagna et al. [6] investigated the production of Egyptian green pigments and analyzed the chemical and structural properties of raw Egyptian blue and green pigment cakes and pigment samples taken from paintings kept in the Louvre Museum, France. In their research, they took into account the role of firing temperature, atmospheric conditions in the furnace, and cooling rate. Demidenko et al. [11] investigated the microstructure of a material based on natural wollastonite at different sintering temperatures ranging from 850 °C to 1100 °C. They also studied the effect of microstructure on the porosity, shrinkage, water absorption, and mechanical strength.

Pagés-Camagna et al. [12] studied the Egyptian blue and green pigments in archaeological samples using Scanning Electron Microscopy (SEM) images and Raman spectroscopy. They could finally identify tenorite (CuO), confirming that the synthesis of both pigments could be performed in an oxidizing atmosphere. In another research, Pagés-Camagna et al. [13] reported some valuable information on the coloring mechanism of Egyptian blue and green pigments.

Dabanlı et al. [14] investigated the samples of glazed tiles belonging to a monument located in Southeastern Anatolia. They concluded that alkali and lead oxides were the main components of glazes along with small amounts of lead oxide. They also found that the blue/green turquoise colors were obtained from copper while the blue pigment itself was derived from cobalt. Omar [15] investigated the body and glaze layer of the Sapil (public fountain) and Kuttab (school) of Mustafa Sinan monuments. The results from tiles analysis proved the application of local clay mixed with a small amount of lime. They also stated that the alkaline and lead oxides were the main components of the glaze layer with high amount of lead oxide in samples. In addition, the obtained results confirmed the presence of copper oxide contributing to the creation of light blue and green color in the samples under study.

In this research, six samples obtained from green-blue glazed ancient ceramic tiles from Abdolazim Hasani Shrine, Ray, Iran, inherited from the Safavid era (1501-1736) were collected to identify the chemical compositions and nature of their pigments through analytical techniques. In characterizing ancient colored glazes, the pigments in the glaze were identified and investigated through different analytical methods based on available scientific references. The main objective of this study was to determine whether or not the nature of green-blue color pertained to the Egyptian blue.

2. MATERIALS AND METHODS

2.1. Materials

Six green-blue glazed samples, shown in Figure 1, were collected from ancient potteries belonging to the Safavid era from different parts of Abdolazim Hasani Shrine, Ray, Iran.

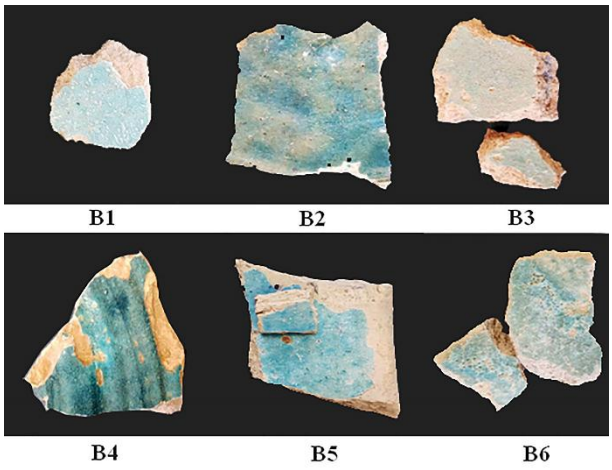

Figure 1. The glazed samples from different parts of Abdolazim Hasani Shrine

2.2. Methods

Followed by collecting the samples, a thin layer of glaze was mechanically removed from their surfaces. The chemical compositions of the samples were analyzed using X-Ray Probe Micro Analyzer (XPMA, HORIBA XGT7200). In addition, the phase composition was characterized through X-ray Diffraction (XRD, Panalytical Expert) method using Cu Kα radiation (λ=1.54 Å). The microscopic studies were performed using SEM (FEI ESEM QUANTA 200) coupled with Energy Dispersive X-ray spectroscopy (EDS, EDAX EDS Silicon Drift, 2017) using Backscattered Electron Emission (BSE). Raman studies on the colored glazed samples were carried out using Confocal Raman Microscope (Xplora Plus, Horiba Co., France). In addition, FTIR studies were carried out using PerkinElmer spectrometer (Spectrum One FTIR, USA). The reflectance spectra were recorded using a 4500L Hunter Lab Mini Scan EZ spectrophotometer. The chromatic values were then expressed as CIE L*a*b*color coordinates under D65/10º Illuminant in the spectral range of 400-700 nm.

Considerations of the Raman spectroscopy calibration were as follows:

Part 1- Calibrating the zero-order position:

The ZERO parameter changed in small increments, e.g., +5 or -5 at a time, considered as the number of nm moving per motor.

Part 2- Calibrating the Raman spectrum:

This calibration stage was done using a known emission line from a Mercury or Neon lamp. Then, the Laser wavelength was altered, and the XY stage movement and Laser Spot Position were calibrated. Finally, the required software for data analysis was installed.

3. RESULTS AND DISCUSSION

3.1. Chemical Composition

Table 1 presents the results from the XPMA analysis (chemical compositions of the elements in glaze samples, and Figure 2 lists the concentration values of the detected elements (in wt. % of their oxides) in Samples B1-B6.

In addition to creating a white hue color, CaO can increase the resistance of the glaze matrix to water, acid, and surface scratches. It also improves the adhesion of glaze to the substrate. It is well known that the copper oxide in ceramics usually creates a green shade; however, in the presence of alkaline and alkaline earth metal oxides such as calcium oxide, potassium oxide, and sodium oxide, it produces blue and green-blue shades [16].

As observed, SiO_2 is the main phase in all samples along with Al_2O_3, Cu_2O, as well as alkaline and alkaline earth metal oxides (i.e. CaO and Na_2O, and K_2O).

TABLE 1. The chemical composition of the elements in the glaze samples B1-B6. The magnitude is as wt. %

	B1	B2	B3	B4	B5	B6
Na_2O	-	13.59	11.94	0.00	0.00	12.64
MgO	0.01	0.01	0.03	0.03	0.00	0.02
Al_2O_3	5.40	3.22	3.58	7.87	2.01	4.89
SiO_2	81.60	73.77	71.46	76.40	85.18	72.54
SO_3	0.18	0.15	0.28	0.15	0.02	0.16
K_2O	1.24	3.35	2.55	3.80	4.49	2.70
CaO	9.87	4.95	8.39	7.10	5.71	5.48
TiO_2	0.02	0.03	0.04	0.03	0.01	0.04
MnO_2	0.06	0.14	0.14	0.06	0.06	0.04
Fe_2O_3	0.18	0.14	0.55	0.17	0.07	0.27
CuO	1.12	0.60	1.00	3.69	1.33	1.18
ZnO	0.10	0.00	0.00	0.06	0.04	0.00
SrO	0.05	0.04	0.04	0.04	0.03	0.05
PbO	0.16	0.00	0.00	0.61	1.09	0.00

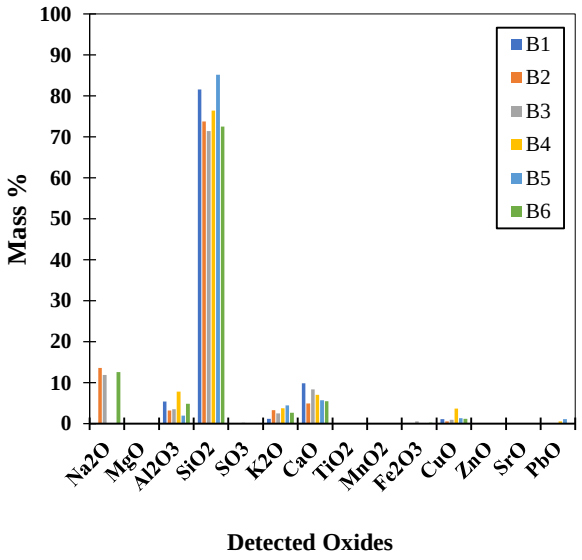

Figure 2. XPMA results demonstrating the concentrations of the detected elements in Samples B1-B6

3.2. X-Ray Diffraction

Table 2 summarizes the main phases identified from the XRD patterns of Samples B1-B6, and Figure 3 demonstrates the XRD Pattern of the ancient colored glazed Samples B1-B6.

TABLE 2. Detected phases in Samples B1-B6

Sample	Main Phases	Chemical Formula
B1	No crystalline phase	-
B2	No crystalline phase	-
B3	Wollastonite, Quartz, lime	$CaSiO_3$, SiO_2, CaO
B4	Wollastonite	$CaSiO_3$
B5	Quartz, lime, Cristobalite	SiO_2, CaO,SiO_2
B6	Quartz, Cristobalite	SiO_2, SiO_2

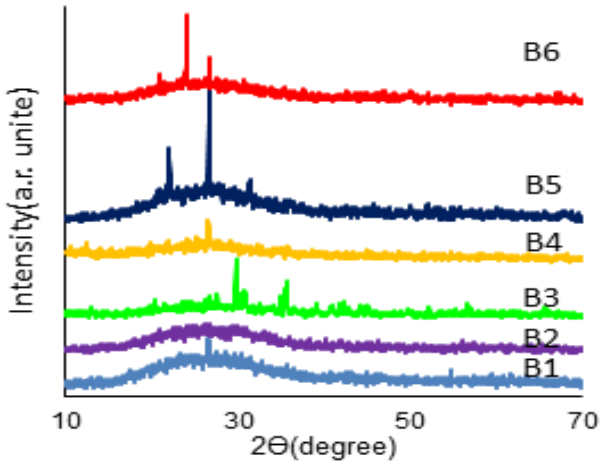

Figure 3. XRD Pattern of the ancient colored glazed Samples B1-B6

While no crystalline phases are observed in the XRD patterns of these samples, three mineral phases of lime, quartz, and wollastonite (calcium silicate) were detected in Sample B3. According to the findings, Sample B4 was only composed of wollastonite phase B3. The presence of wollastonite in the colored glazes can be important evidence for the presence of Egyptian green pigments in the glaze formulation [6,10,16]. The XRD patterns of Samples B5 and B6 also confirm the presence of quartz, lime, and cristobalite. However, the wollastonite phase in these samples was not detected due to its low concentration. As mentioned in the methodology section, the procedure of the separation of glaze from the surface of ceramics was in such a way that the adhesion of the body to the glaze should be probable. This is why some parts of glaze are crystalline while some others are not.

As reported by Pagés-Camagna et al. [6], Egyptian green glazes must have been fired at higher temperatures than Egyptian blue ones. As a result, the cristobalite phase can be identified in the Egyptian green glazes. In other words, cristobalite can be the considered as a main characteristic of Egyptian green [6,10,16].

3.3. Microstructure

Figure 4 demonstrates the SEM images of the six samples according to which, the samples are porous with heterogeneous microstructure. Small white pigment particles (0.6 µm for samples B1 and B6, 1.25 µm for samples B2 and B5, 4.5 µm for sample B4, and 5.5 µm for sample B3) are recognizable on the surface of the glaze that was eroded due to the aging and long-term exposure to severe environmental conditions such as wind. In Sample B3, the glaze surface has many bubbles, hence not uniform, and there is a significant difference between the erosion of the glaze matrix and that of other phases such as quartz and wollastonite. Samples B1 and B2, however, have a relatively uniform eroded surface. Higher degrees of erosion is observed on the surface of Samples B3 to B6 probably due to the presence of crystalline phases in the glazed ceramic tiles.

SEM-EDS results for the glaze matrix and white particles (shown as white spots in Figure 4) are presented in Tables 3 and 4, respectively.

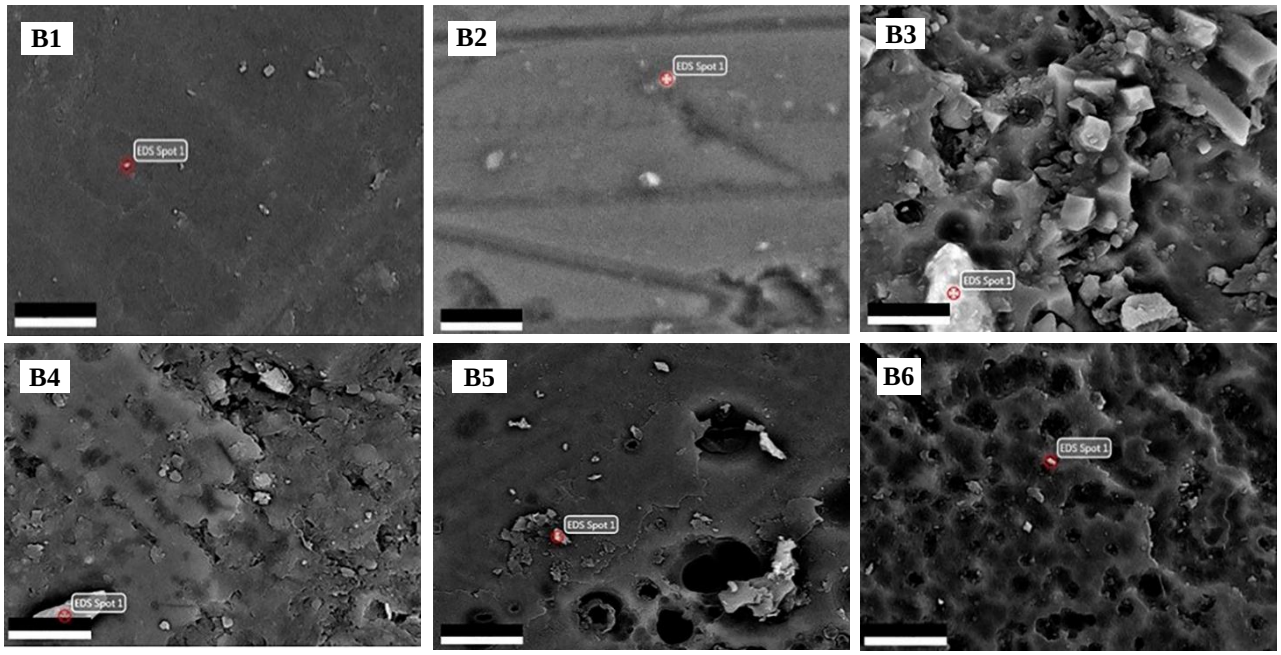

Figure 4. Back-scattered SEM images of the glazed samples at 5000X. EDS spots are shown in each image. The scale bar is 5 µm

TABLE 3. EDS analysis of the glaze matrix (wt. %)

Sample	O	Na	Mg	Al	Si	K	Ca	Fe	Cu	Sn
B1	23.55	3.29	1.41	3.62	50.89	2.46	7.71	3.78	3.28	-
B2	25.27	9.49	2.44	2.84	45.25	4.81	6.07	1.31	2.52	-
B3	29.94	4.66	3.78	3.3	38.85	2.5	9.79	4.53	2.64	-
B4	28.58	5.03	3.62	5.74	39.58	3.69	4.99	2.27	6.5	-
B5	27.2	4.83	1.86	2.47	46.29	6.24	6.93	0.94	3.24	-
B6	20.95	7.6	1.94	3.1	49.62	3.92	5.93	1.79	5.14	-
Average	25.9	5.8	2.5	3.5	45.1	3.9	6.9	2.4	3.9	-
Standard Deviation	3.3	2.3	1.0	1.2	5.0	1.4	1.7	1.4	1.6	-

TABLE 4. EDS analysis of white particles shown in the SEM images in Figure 4 (wt. %)

Sample	O	Na	Mg	Al	Si	K	Ca	Fe	Cu	Sn
B1	25.1	8.4	4.3	3.2	46.3	1.6	6.8	1.0	2.1	-
B2	24.8	10.0	3.3	2.9	36.6	2.9	4.1	13.3	2.0	-
B3	12.4	4.8	1.2	1.5	20.4	1.0	3.4	1.6	1.4	52.3
B4	31.6	6.9	4.4	5.0	38.6	2.9	5.1	2.0	3.5	-
B5	33.5	6.1	2.6	3.5	41.1	4.6	5.2	0.81	2.6	-
B6	30.3	8.8	3.1	3.5	36.4	2.7	10.9	1.1	3.3	-
Average	26.3	7.5	3.1	3.3	36.6	2.6	5.9	1.6	2.6	26.3
Standard Deviation	7.7	1.9	1.2	1.1	8.7	1.2	2.7	1.0	0.8	7.7

The average and standard deviations are also compared in Figure 5. According to this figure, the glazes are silica-based containing different amounts of silicon from 38.85 to 50.89 wt. % for Samples B3 and B1, respectively. The glazes also contain other alkaline and alkaline earth elements such as calcium, sodium, and potassium. Copper was also detected in all the samples ranging from 2.52 wt. % for sample B2 to 6.5 wt. % for sample B4.

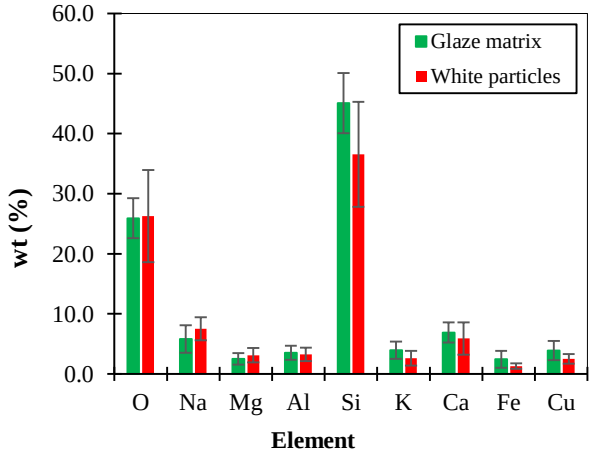

Figure 5. Comparison between the average and standard deviations of different elements in the glaze matrix and white particles, as listed in tables 3 and 4

According to Figure 5, the concentration of silicon in the white particles (46.34 wt. %) is lower than that in the glaze matrix (e.g. for sample B1, 46.34 wt. % and 50.89 wt. %, respectively). The same trend was also observed for Al, K, Ca, Fe, and Cu elements in all six samples. The higher Fe content of white particles in Sample B2 is inicative of the fabrication of this pigment using iron-rich raw materials

Sample B3 contained high concentration of tin (52.34 wt. %) probably due to the presence of tin in the copper source (e.g., tin bronze). Oudbashi et al. [17] also reported the presence of tin element in their samples. White particles in Sample B6 contained calcium with high concentration of about 10.86 % which may be attributed to the utilization of Ca-rich raw materials such as calcite ($CaCO_3$) or CaO in the fabrication of this pigment.

The distribution of the constituents in the glaze matrix and white particles was also investigated for Sample B2, as a representative sample, using line scan and element profile plot, as shown in Figure 6.

As observed, while moving from point A to point B, the concentration of Si (in wt. %) decreased until reaching a white particle and then increased again in the Si-rich matrix. Since white particle is supposed to be an Egyptian green pigment (calcium silicate), the silicon concentration decreased while those of Ca and O increased. Evidently, copper has uniform distribution throughout the sample (i.e., both glaze matrix and white particles). The same trend was observed for these elements in other five samples that are not shown here.

The CaO/CuO ratio can be caluclated using SEM-EDS analysis of bulk compositions of the glazed samples given in Table 5 where it is observed that the bulk lime concentration is normally greater than that of the bulk copper oxide. Of note, the CaO/CuO ratio is greater than 1.5. However, due to loss of material through weathering and possible contamination during ancient discoveries, the differences in the CaO/CuO ratios are less explicit in some samples. The obtained results are in accordance with the results obtained by Hatton et al. [18].

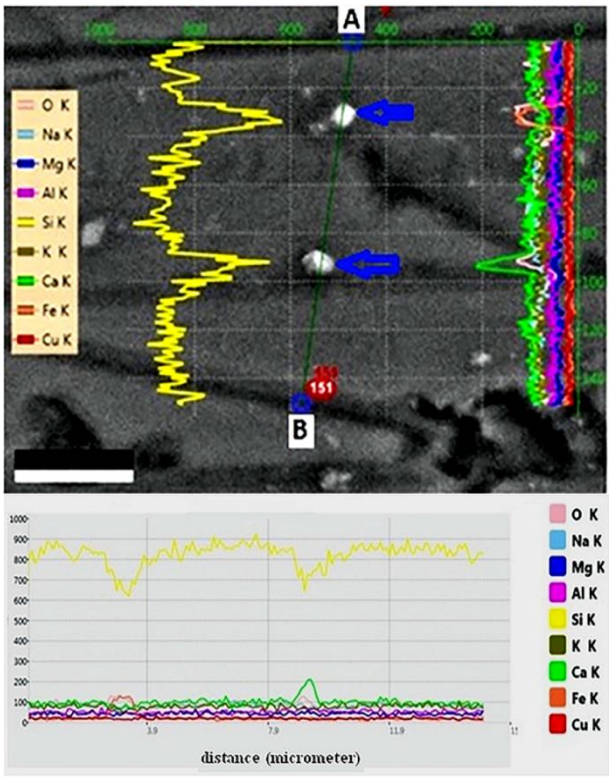

Figure 6. Line scan and element profile plot of glaze matrix and white particles for B2 sample

Another noticeable feature is that these samples contain high concentration of soda (Na_2O). Moreover, in this research, the green-blue colored glaze samples are characterized by high flux concentrations, i.e., Na_2O plus K_2O between 5.3 % and 14.1 %, respectively, in Samples B1 and B2. This result is also in agreement with the results obtained by Pagés-Camagna et al. [6].

3.4. Raman Spectroscopy

Raman spectroscopy was used for the characterization of the ancient green-blue glazed samples. It is a reliable, fast, sensitive and nondestructive test method which measures different vibrational modes, thus providing complementary information on the analyzed materials. Figure 7 shows the Raman spectroscopy spectra of the glazed samples. Two weak bands are observed at 150 cm^{-1} and 180 cm^{-1} mainly due to the presence of chalk [19] and gypsum [20], respectively. The peak at around 260 cm^{-1} is attributed to the wollastonite crystalline phase [21] which is usually found in Egyptian green pigment used in the ancient glazed ceramic tiles. The weak bands around 406 cm^{-1}, 391 cm^{-1}, and 253 cm^{-1} are also attributed to ν(Cu-Cl) stretching [22], ν(O-Cu-O) symmetric stretching, and ν(O-Cu-O) bending [23], respectively. The bands at around 300 cm^{-1} and 360 cm^{-1} correspond to copper oxide [24] while those around at 350 cm^{-1} and 380 cm^{-1} belong to quartz [25-27]. In addition, the band around at 360 cm^{-1} is attributed to calcite [28,29].

There are two bands at around 425 cm^{-1} and 460 cm^{-1} which can be attributed to the tridymite [21] and quartz [25-29], respectively. Bianchetti et al. [8] reported that tridymite was a dominant crystalline phase in the Egyptian green pigment that was produced at temperatures higher than 950 ºC.

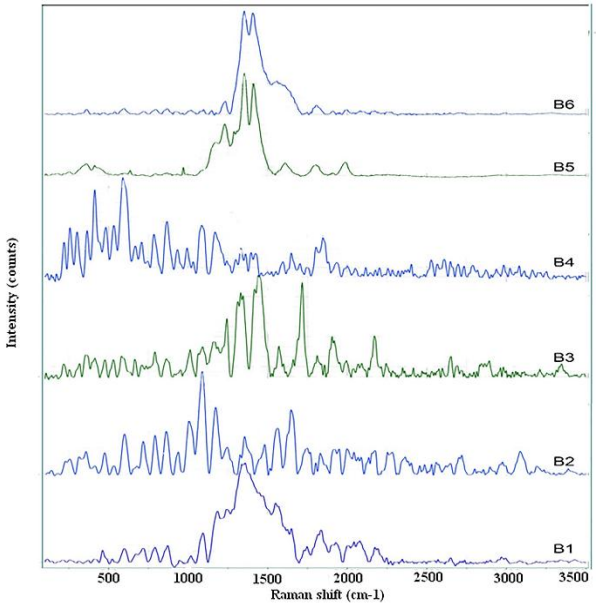

Figure 7. Raman spectra of the B1-B6 glazed samples

The two bands at around 470 cm^{-1} and 750 cm^{-1} in Sample B3 is associated with the SnO_2 [30] due to the presence of about 52.34 wt. % tin in white particles. In addition, there are other weak and medium bands at around 540 cm^{-1} and 710 cm^{-1} which belong to the green earth [31] while those at 590 cm^{-1} and 600 cm^{-1} correspond to the Egyptian green [20,32] and copper oxide [24], respectively. Raman bands at around 717 cm^{-1}, 780cm^{-1} , 865 cm^{-1}, 930 cm^{-1}, and 940 cm^{-1} are attributed to the calcite [28, 29], tridymite [21], allophone [33,34], and chrysocolla [35], respectively.

In contrast to the XRD patterns according to which, cristobalite phase was only detected in Samples B5 and B6, this phase was found in Samples B1-B6 according to Raman bands at around 410 cm^{-1}, 420 cm^{-1}, 598 cm^{-1}, 780 cm^{-1}, 790 cm^{-1}, and 1075 cm^{-1} [36-38], respectively, thus confirming the presence of the Egyptian green pigment in the formulation of all the investigated ancient glazed ceramic tiles. The bands at 1020 cm^{-1}, 1085 cm^{-1}, and 1170 cm^{-1} can be attributed to the wollastonite [32], calcite [28-29], and quartz [26-29], respectively.

Moreover, the Raman bands at around 1235 cm^{-1}, 1356 cm^{-1}, and 1458 cm^{-1} correspond to the Green earth [31]. The weak and medium peaks at around 1445 cm^{-1} and 1550 cm^{-1} may also be attributed to the Verdigris [39]

TABLE 5. Bulk Chemical compositions of green-blue colored glaze samples (EDS analysis normalized to 100 %)

Sample Code	SiO_2	CuO	CaO	Na_2O	K_2O	MgO	Al_2O_3	Fe_2O_3	CaO/CuO
B1	62.99	3.14	5.82	2.64	2.69	0.96	13.43	8.31	1.85
B2	61.62	2.65	5.04	8.39	5.78	1.72	11.59	3.17	1.89
B3	53.95	2.83	8.30	4.20	3.06	2.73	13.74	11.17	2.92
B4	51.12	2.60	3.94	4.22	4.21	2.43	22.26	5.21	1.51

while the band at around 1480 cm^{-1} results from the vibration stretching of C-C bond [40]. Of note, the Raman bands at around 17549 cm^{-1} and 1940 cm^{-1} may be attributed to C-O vibration stretching [41] while the band at around 1645 cm^{-1} can be associated with the OH stretching mode in water. Moreover, the Raman bands in the range of 2000-4000 cm^{-1} are attributed to the vibration stretching of hydroxyl and water [42,43].

3.5. Colorimetry

Figure 8 and Table 6 present the reflectance spectra and CIE L*a*b* values of the studied ancient glazed ceramic tiles, respectively. Table 6 also lists the average values of a* and b*. As observed in Figure 8, there is a high intensity reflectance spectrum in the range of 490-560 nm. Therefore, it can be concluded that the samples are green with different hues.

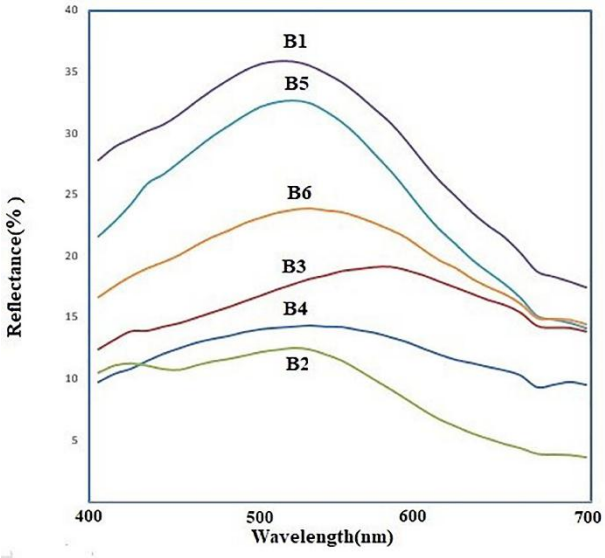

Figure 8. Reflectance spectra of the green-blue glazed samples

TABLE 6. Colorimetric parameters (L*a*b*) of the ancient glazed ceramic tiles based on D65 observer

Sample	L*	a*	b*	c	Cu (wt. %)
B1	63.53	-10.49	0.44	10.5	3.28
B2	38.39	-11.78	-2.41	12.03	2.52
B3	49.47	-2.45	7.15	7.55	2.64
B4	43.48	-5.38	2.7	6.02	6.5
B5	60.47	-12.47	1.31	12.54	3.24
B6	54.27	-6.95	3.67	7.86	5.14

The copper concentration in the raw material plays an important role in achieving better green shades (higher a* and c* values) in these glazes. For example, c* = 12.5 and c* = 10.5 were obtained for 3.2 wt. % and 3.3 wt. % copper in Sample B5 and B1, respectively. On the contrary, Cu contents higher than this value (3.3) produce a poor green shade (e.g. c* = 6 and c* = 7.86 for 6.5 wt. % and 5.14 wt. % copper in Samples B4 and B6. The same results were obtained for copper contents lower than 3.3 wt. % (for example, in Sample B3). In Sample B2 (Cu = 2.52 wt. % and c* = 12.03), however, the pigment is Egyptian blue since b* = -2.41. To be specific, the green color is produced due to the presence of Cu^{2+} metallic ion in an octahedral structure in the amorphous silica-rich matrix [44].

4. CONCLUSION

In this research, six green-blue ancient glazed ceramic tiles collected from Abdolazim Hasani Shrine, Ray, Iran, were investigated using the XPMA, XRD, FTIR, and Raman spectroscopy. The obtained results confirmed the presence of three main phases of tridymite, cristobalite, and wollastonite, the main constituents of Egyptian green pigments. Colorimetry analysis confirmed that the presence of Cu^{2+} ion in an octahedral structure within amorphous silica-rich matrix was responsible for the observed green hue. In addition, the SEM-EDS revealed the uniform and homogeneous distribution of copper throughout the glaze matrix.

ACKNOWLEDGEMENTS

We would like to express our gratitude to Iran National Science Foundation (INSF) for supporting this research under grant no. 98027092, and from Institute for color science and technology (ICRC) who provided facilities that greatly assisted the research.

REFERENCES

1. Mokhtarshahi Sani, R., "A Conceptual Understanding for Teaching the History of Islamic Architecture: An Iranian (Persian) Perspective", ***International Journal of Architectural Research***, Vol. 3, No. 1 , (2009), 233-244. https://www.researchgate.net/publication/26597708_A_Conceptual_Understanding_for_Teaching_the_History_of_Islamic_Arch

itecture_An_Iranian_Persian_Perspective/fulltext/0e605659f0c46d4f0ab1bf3e/A-Conceptual-Understanding-for-Teaching-the-History-of-Islamic-Architecture-An-Iranian-Persian-Perspective.pdf?origin=publication_detail
2. Delamare, F., "Sur les processus physiques intervenant lors de la synthèse du bleu égyptien: Réflexion à propos de la composition de pigments bleus gallo-romains", ***ArchéoSciences, revue d'Archéométrie***, Vol. 21, No. 1, (1997), 103-119. https://doi.org/10.3406/arsci.1997.952
3. Eastaugh, N., Walsh, V., Chaplin, T., Siddall, R., ***Pigment Compendium: A Dictionary and Optical Microscopy of Historical Pigments***, Burlington, VT, Butterworth-Heinemann, (2008). https://doi.org/10.4324/9780080943596
4. Scott, D. A., ***Copper and Bronze in Art: Corrosion, Colorants, Conservation***, Getty Publications, (2002). https://www.getty.edu/publications/virtuallibrary/temp/9780892366385.pdf
5. Wiedemann, H. G., Bayer, G., "The bust of Nefertiti", ***Analytical Chemistry***, Vol. 54, No. 4, (1982), 619A-628A. https://doi.org/10.1021/ac00241a790
6. Pagés-Camagna, S., Colinart, S., "The Egyptian Green pigment: Its manufacturing process and links to Egyptian Blue", ***Archaeometry***, Vol. 45, No. 4, (2003), 637-658. https://doi.org/10.1046/j.1475-4754.2003.00134.x
7. Ullrich, D., "Egyptian Blue and Green Frit: Characterization, History and Occurrence, Synthesis", In ***Pact***, Vol. 17, No. II.3.1, (1987), 323-332. http://www.univeur.org/cuebc/downloads/Pubblicazioni%20scaricabili/PACT%2017%20-%20Datation-Caract%C3%A9risation%20des%20peintures%20pari%C3%A9tales%20et%20murales/16%20Ullrich.pdf
8. Bianchetti, P., Talarico, F., Viglianoa, M. G., Ali, M. F., "Production and characterization of Egyptian blue and Egyptian green frit", ***Journal of Cultural Heritage***, Vol. 1, No. 2, (2000), 179-188. https://doi.org/10.1016/S1296-2074(00)00165-5
9. Abdel-Ghani, M. H., ***A Multi-Instrument Investigation of Pigments, Binders and Varnishes from Egyptian Paintings (AD 1300-1900): Molecular and Elemental Analysis Using Raman, GC-MS and SEM-EDX Techniques***, Doctoral dissertation, University of Bradford, (2009). http://hdl.handle.net/10454/4315
10. Gražėnaitė, E., Kiuberis, J., Beganskienė, A., Senvaitienė, J., Kareiva, A., "XRD and FTIR characterization of historical green pigments and their lead-based glazes", ***Chemija***, Vol. 25, No. 4, (2014), 199–205. http://mokslozurnalai.lmaleidykla.lt/publ/0235-7216/2014/4/199%E2%80%93205.pdf
11. Demidenko, N. I., Tel'nova, G. B., "Microstructure and properties of a material based on natural wollastonite", ***Glass and Ceramics***, Vol. 61, No. 5-6, (2004), 183-186. https://doi.org/10.1023/B:GLAC.0000043088.65135.11
12. Pagès-Camagna, S., Colinart, S., Coupry, C., "Fabrication Processes of Archaeological Egyptian Blue and Green Pigments Enlightened by Raman Microscopy and Scanning Electron Microscopy", ***Journal of Raman Spectroscopy***, Vol. 30, No. 4, (1999), 313-317. https://doi.org/10.1002/(SICI)1097-4555(199904)30:4<313::AID-JRS381>3.0.CO;2-B
13. Pagès-Camagna, S., Reiche, I., Brouder, C., Cabaret, D., Rossano, S., Kanngießer, B., Erko, A., "New insights into the color origin of archaeological Egyptian blue and green by XAFS at the Cu K-edge", ***X-Ray Spectrometry: An International Journal***, Vol. 35, No. 2, (2006), 141-145. https://doi.org/10.1002/xrs.885
14. Dabanlı, Ö., Yıldız, D., Bayazit, M., "Composition and Phase Analysis On Glazed Tiles of Southeast Anatolia: Production Process Identification", ***Mediterranean Archaeology & Archaeometry***, Vol. 21, No. 3, (2021), 1-22. https://doi.org/10.5281/zenodo.5545709
15. Omar, S., "Characterization of The Ottoman Ceramic Tiles in the Facade of Mustafa Sinans Sapil (Cairo, Egypt)", ***Scientific Culture***, Vol. 8, No. 2, (2022), 1-15. https://doi.org/10.5281/zenodo.6323156
16. Mahmoud, H. M., Papadopoulou, L., "Archaeometric Analysis of Pigments from the Tomb of Nakht-Djehuty (TT189), El-Qurna Necropolis, Upper Egypt", ***ArcheoSciences, Revue d'archéométrie***, Vol. 37, (2013), 19-33. https://doi.org/10.4000/archeosciences.3967
17. Oudbashi, O., Hessari, M., "A "western" imported technology: An analytical study of the Achaemenid Egyptian blue objects", ***Journal of Cultural Heritage***, Vol. 47, (2021), 246-256. https://doi.org/10.1016/j.culher.2020.11.001
18. Hatton, G. D., Shortland, A. J., Tite, M. S., "The production technology of Egyptian blue and green frits from second millennium BC Egypt and Mesopotamia", ***Journal of Archaeological Science***, Vol. 35, No. 6, (2008), 1591-1604. https://doi.org/10.1016/j.jas.2007.11.008
19. Ion, R. M., Turcanu-Caruţiu, D., Fierăscu, R. C., Fierăscu, I., Bunghez, I. R., Ion, M. L., Teodorescu, S., Vasilievici, G., Rădiţoiu, V., "Caoxite-hydroxyapatite composition as consolidating material for the chalk stone from Basarabi–Murfatlar churches ensemble", ***Applied Surface Science***, Vol. 358, (2015), 612-618. https://doi.org/10.1016/j.apsusc.2015.08.196
20. Charola, A. E., Pühringer, J., Steiger, M., "Gypsum: a review of its role in the deterioration of building materials", ***Environmental Geology***, Vol. 52, No. 2, (2007), 339-352. https://doi.org/10.1007/s00254-006-0566-9
21. Coccato, A., Bersani, D., Coudray, A., Sanyova, J., Moens, L., Vandenabeele, P., "Raman spectroscopy of green minerals and reaction products with an application in Cultural Heritage research", ***Journal of Raman Spectroscopy***, Vol. 47, No. 12, (2016), 1429-1443. https://doi.org/10.1002/jrs.4956
22. Frost, R. L., Martens, W., Kloprogge, J. T., Williams, P. A., "Raman spectroscopy of the basic copper chloride minerals atacamite and paratacamite: implications for the study of copper, brass and bronze ceramic tiles of archaeological significance", ***Journal of Raman Spectroscopy***, Vol. 33, No. 10, (2002), 801-806. https://doi.org/10.1002/jrs.921
23. Liu, X. D., Hagihala, M., Zheng, X. G., Guo, Q. X., "Vibrational spectroscopic properties of botallackite-structure basic copper halides", ***Vibrational Spectroscopy***, Vol. 56, No. 2, (2011), 177-183. https://doi.org/10.1016/j.vibspec.2011.02.002
24. Deng, Y., Handoko, A. D., Du, Y., Xi, S., Yeo, B. S., "In Situ Raman Spectroscopy of Copper and Copper Oxide Surfaces during Electrochemical Oxygen Evolution Reaction: Identification of CuIII Oxides as Catalytically Active Species", ***Acs Catalysis***, Vol. 6, No. 4, (2016), 2473-2481. https://doi.org/10.1021/acscatal.6b00205
25. Gillet, P., Le Cléac'h, A., Madon, M., "High-temperature raman spectroscopy of SiO_2 and GeO_2 Polymorphs: Anharmonicity and thermodynamic properties at high-temperatures", ***Journal of Geophysical Research: Solid Earth***, Vol. 95, No. B13, (1990), 21635-21655. https://doi.org/10.1029/JB095iB13p21635
26. Gillet, P., "Raman spectroscopy at high pressure and high temperature. Phase transitions and thermodynamic properties of minerals", ***Physics and Chemistry of Minerals***, Vol. 23, No. 4, (1996), 263-275. https://doi.org/10.1007/BF00207767
27. Hemley, R. J., "Pressure Dependence of Raman Spectra of SiO_2 Polymorphs: α-Quartz, Coesite, and Stishovite", In Manghnani, M. H. and Syono, Y. (Eds.), ***High-Pressure Research in Mineral Physics: A Volume in Honor of Syun-iti Akimoto***, Tokyo, Terra Scientific Publishing Company (TERRAPUB), Washington D.C., American Geophysical Union, Vol. 39, (1987), 347-359. https://doi.org/10.1029/GM039p0347
28. De La Pierre, M., Carteret, C., Maschio, L., André, E., Orlando, R., Dovesi, R., "The Raman spectrum of $CaCO_3$ polymorphs calcite and aragonite: A combined experimental and computational study", ***The Journal of Chemical Physics***, Vol. 140, No. 16, (2014), 164509. https://doi.org/10.1063/1.4871900
29. Gunasekaran, S., Anbalagan, G., Pandi, S., "Raman and infrared spectra of carbonates of calcite structure", ***Journal of Raman Spectroscopy***, Vol. 37, No. 9, (2006), 892-899. https://doi.org/10.1002/jrs.1518
30. Herrera, L. K., Videla, H. A., "Surface analysis and materials characterization for the study of bio deterioration and weathering

effects on cultural property", ***International Biodeterioration & Biodegradation***, Vol. 63, No. 7, (2009), 813-822. https://doi.org/10.1016/j.ibiod.2009.05.002
31. Ospitali, F., Bersani, D., Di Lonardo, G., Lottici, P. P., "'Green earths': vibrational and elemental characterization of glauconites, celadonites and historical pigments", ***Journal of Raman Spectroscopy***, Vol. 39, No. 8, (2008), 1066-1073. https://doi.org/10.1002/jrs.1983
32. Huang, E., Chen, C. H., Huang, T., Lin, E. H., Xu, J. A., "Raman spectroscopic characteristics of Mg-Fe-Ca pyroxenes", ***American Mineralogist***, Vol. 85, No. 3-4, (2000), 473-479. https://doi.org/10.2138/am-2000-0408
33. Bishop, J. L., Ethbrampe, E. B., Bish, D. L., Abidin, Z. L., Baker, L. L., Matsue, N., Henmi, T., "Spectral and Hydration Properties of Allophane and Imogolite", ***Clays and Clay Minerals***, Vol. 61, No. 1, (2013), 57-74. https://doi.org/10.1346/CCMN.2013.0610105
34. Friedlander, L. R., Glotch, T. D., Bish, D. L., Dyar, M. D., Sharp, T. G., Sklute, E. C., Michalski, J. R., "Structural and spectroscopic changes to natural non tronite induced by experimental impacts between 10 and 40GPa", ***Journal of Geophysical Research: Planets***, Vol. 120, No. 5, (2015), 888-912. https://doi.org/10.1002/2014JE004638
35. Derbyshire, A., Withnall, R., "Pigment analysis of portrait miniatures using Raman microscopy", ***Journal of Raman Spectroscopy***, Vol. 30, No. 3, (1999), 185-188. https://doi.org/10.1002/(SICI)1097-4555(199903)30:3<185::AID-JRS357>3.0.CO;2-U
36. Bates, J. B., "Raman Spectra of α and β Cristobalite", ***The Journal of Chemical Physics***, Vol. 57, No. 9, (1972), 4042-4047. https://doi.org/10.1063/1.1678878
37. Kingma, K. J., Heymley, R. J., "Raman spectroscopic study of microcrystalline silica", ***American Mineralogist***, Vol. 79, No. 3-4, (1994), 269-273. https://eurekamag.com/research/019/844/019844826.php
38. Liang, Y., Miranda, C. R., Scandolo, S., "Infrared and Raman spectra of silica polymorphs from an ab initio parametrized polarizable force field", ***The Journal of Chemical Physics***, Vol. 125, No. 19, (2006), 194524. https://doi.org/10.1063/1.2390709
39. San Andrés, M., De la Roja, J. M., Baonza, V. G., Sancho, N., "Verdigris pigment: a mixture of compounds. Input from Raman spectroscopy", ***Journal of Raman Spectroscopy***, Vol. 41, No. 11, (2010), 1468-1476. https://doi.org/10.1002/jrs.2786
40. Shenderova, O. A., Gruen, D. M., ***Ultrananocrystalline Diamond: Synthesis, Properties, and Applications***, 2nd Ed., Norwich, New York, William Andrew, (2012). https://doi.org/10.1016/C2010-0-67069-6
41. Xu, W., Sun, Y., Dong, X., Li, S., Wang, H., Xue, J., Zheng, X., "Local order and vibrational coupling of the C=O Stretching Mode of γ-Caprolactone in liquid binary mixtures", ***Scientific Reports***, Vol. 7, No. 1, (2017), 12182. https://doi.org/10.1038/s41598-017-12030-1
42. Sergeeva, A. V., Zhitova, E. S., Nuzhdaev, A. A., Zolotarev, A. A., Bocharov, V. N., Ismagilova, R. M., "Infrared and Raman Spectroscopy of Ammoniovoltaite, $(NH_4)_2Fe^{2+}{}_5Fe^{3+}{}_3Al(SO_4)_{12}(H_2O)_{18}$", ***Minerals***, Vol. 10, No. 9, (2020), 781. https://doi.org/10.3390/min10090781
43. Kolesov, B., "Raman investigation of H_2O molecule and hydroxyl groups in the channels of hemimorphite", ***American Mineralogist***, Vol. 91, No. 8-9, (2006), 1355-1362. https://doi.org/10.2138/am.2006.2179
44. Keppler, H., "Crystal field spectra and geochemistry of transition metal ion in silicate melts and glasses", ***American Mineralogist***, Vol. 77, No. 1-2, (1992), 62-75. http://www.minsocam.org/ammin/AM77/AM77_62.pdf